

# Efficient seismic reliability and fragility analysis of lifeline networks using subset simulation

Dongkyu Lee<sup>a</sup>, Ziqi Wang<sup>b</sup>, Junho Song <sup>\*a</sup>

<sup>a</sup>*Department of Civil and Environmental Engineering, Seoul National University, Seoul, Republic of Korea*

<sup>b</sup>*Department of Civil and Environmental Engineering, University of California, Berkeley, CA, USA*

---

## Abstract

Various simulation-based and analytical methods have been developed to evaluate the seismic fragilities of individual structures. However, a community's seismic safety and resilience are substantially affected by network reliability, determined not only by component fragilities but also by network topology and commodity/information flows. However, seismic reliability analyses of networks often encounter significant challenges due to complex network topologies, interdependencies among ground motions, and low failure probabilities. This paper proposes to overcome these challenges by a variance-reduction method for network fragility analysis using subset simulation. The binary network limit-state function in the subset simulation is reformulated into more informative piecewise continuous functions. The proposed limit-state functions quantify the proximity of each sample to a potential network failure domain, thereby enabling the construction of specialized intermediate failure events, which can be utilized in subset simulation and other sequential Monte Carlo approaches. Moreover, by discovering an implicit connection between intermediate failure events and seismic intensity, we propose a technique to obtain the entire network fragility curve with a single execution of specialized subset simulation. Numerical examples demonstrate that the proposed method can effectively evaluate system-level fragility for large-scale networks.

**Keywords:** Fragility, Lifeline networks, Network reliability, Seismic reliability, Subset simulation

---

## 1. Introduction

Lifeline networks, such as transportation, gas, and electricity systems, are the critical backbone of modern society. Their significance is particularly noticeable in the post-hazard stage because emergency assessment, evacuation, life-saving, and repair operations rely on lifeline networks' functionality. Therefore, it is essential to quantify the network reliability to construct and maintain resilient lifeline networks against seismic hazards. To this end, this paper aims to develop an efficient sampling method to assess the seismic reliability and fragility of networks under various earthquake magnitudes.

To quantify the impact of earthquakes on lifeline networks, various network reliability metrics, e.g., connectivity, flow capacity, and travel time, were proposed [1–4]. For example, connectivity reliability, such as two-terminal or  $k$ -terminal reliability, evaluates network accessibility in terms of the probability that at least one origin-destination (OD) pair remains connected. By contrast, capacity reliability is the probability that the flow capacity between OD pairs surpasses a certain threshold. In transportation networks, this analysis can be combined with traffic demand flow analysis to determine the reliability in terms of travel time [1, 5, 6].

In large-scale networks, however, network reliability analysis can be computationally challenging or even infeasible due to the high computation cost, intricate network topology, or interdependencies between components. To mitigate the computational challenge known as “combinatorial explosion,” various simulation-based approaches [7–9] are extensively used, including the crude/direct Monte Carlo simulation (MCS),

---

\*Corresponding author: [junhosong@snu.ac.kr](mailto:junhosong@snu.ac.kr)

owing to their broad applicability and flexibility. However, the crude MCS has a slow convergence rate of  $\mathcal{O}(N^{-1/2})$ , where  $N$  is the number of random sample points. This slow convergence rate may lead to a prohibitive computation cost in rare event simulations, such as the failures of lifeline networks. Furthermore, analyzing the performance of each sample point is time-consuming in large-scale lifeline networks. Surrogate models for network reliability indices [10–12] have been developed to shorten the computation time. However, these surrogate models entail inherent errors, which can be exacerbated in low-probability events.

Advanced sampling techniques [13–20] can accelerate the probability estimation by sampling in critical regions with higher probabilities. In particular, subset simulation (SS) [13] relaxes the target failure event into nested intermediate failure events, effectively estimating low probabilities with relatively small samples. An essential ingredient of SS is ranking sample points according to their limit-state function values so intermediate failure events can be formulated. However, most network limit-state functions in network reliability analyses have binary or multi-state outputs. This feature poses significant challenges for SS because the sample points outside the failure domain have the same limit-state function value; consequently, the algorithm cannot move toward the failure domain as there is no information to guide the sampling in the correct direction. Ching and Hsu (2007) [3] proposed a continuous limit-state function for network reliability analysis using random walks. However, the computation cost for simulating random walks becomes high in large-scale networks. Chan et al. (2022) [21] suggested adapting the number of sample points and conditional probabilities to avoid sampling the same limit-state function value, but this approach is ineffective for estimating the probability of a rare event.

The primary contribution of this paper is to propose two piecewise continuous reformulations of the binary limit-state function representing network disconnection. These new limit-state functions enable the construction of relaxed, intermediate failure events, readily usable in SS and alternative sequential sampling methods [20, 22]. Since the two reformulations involve trade-offs in accuracy and efficiency, one can select the limit-state function that aligns better with the analysis goals. Another main contribution of this paper is an alternative interpretation of the intermediate failure domains in the context of subset simulation-based network fragility analysis. By discovering an implicit connection between intermediate failure events and earthquake magnitude, a single simulation of SS can generate the entire network fragility curve. The proposed method can be readily extended to analyze  $k$ -terminal reliability and  $k$ -out-of- $N$  reliability (focusing on  $k$ -out-of- $N:G$ , but applicable to  $k$ -out-of- $N:F$ ), which are computationally challenging for non-simulation-based approaches [23, 24].

The paper is structured as follows. Section 2 provides an overview of the seismic network reliability analysis. Section 3 briefly reviews SS, develops informative network limit-state functions, and proposes a computational framework for network fragility analysis. In Section 4, three numerical examples demonstrate the performance of the proposed method. Finally, Section 5 summarizes the paper and provides future research directions.

## 2. Overview of seismic network reliability analysis

### 2.1. Ground motion intensity at network components and failure probabilities

For seismic network reliability analysis, one should first assess the seismic risk of individual components/structures in a network. The seismic failure of a component is defined as the event that the seismic demand exceeds the seismic capacity, both of which are uncertain.

#### 2.1.1. Intensity of ground motions

Various ground-motion intensity measures (IMs), such as peak ground acceleration (PGA), peak ground velocity (PGV), and spectral acceleration ( $S_a$ ), are used to quantify seismic demands. One can either adopt one of these IMs or use multiple IMs [25, 26]. In this paper, PGA is used to quantify the intensity of seismic demand, which can be easily extended to  $S_a$  by interpolation [27, 28]. The attenuation relation of PGA can be expressed as [29, 30]

$$\ln D_i = f(M, R_i, \boldsymbol{\lambda}_i) + \eta + \varepsilon_i, \quad (1)$$

where  $D_i$  is the PGA at site  $i$ ;  $f(\cdot)$ , denoted hereafter as  $\ln \bar{D}_i$ , is the attenuation relation for the PGA at site  $i$  as a function of magnitude  $M$ , the distance from the epicenter to site  $i$ ,  $R_i$ , and a set of other explanatory variables  $\lambda_i$ ; and  $\eta$  and  $\varepsilon_i$  are the inter- and intra-event residuals with zero means and standard deviations  $\sigma_\eta$  and  $\sigma_\varepsilon$ , respectively. Since IMs are generally modeled as lognormal random variables, both residuals  $\eta$  and  $\varepsilon_i$  are assumed to follow normal distributions [31].

Since the components in a single network can be close to each other, their IMs and seismic responses can be highly correlated. Specifically, the Pearson correlation coefficient between the PGAs at sites  $i$  and  $j$  arises from the common variable  $\eta$  and the correlation between the intra-event residuals  $\varepsilon_i$  and  $\varepsilon_j$ . It is often assumed that  $\eta$  and  $\varepsilon_i$  are statistically independent, and the correlation coefficient between  $\varepsilon_i$  and  $\varepsilon_j$  is given as a function of the distance  $\Delta_{ij}$  between the two sites. From Eq.(1), the correlation coefficient between  $\ln D_i$  and  $\ln D_j$  is derived as [31]

$$\rho_{\ln D_i \ln D_j}(\Delta_{ij}) = \frac{\text{Cov}[\ln D_i, \ln D_j]}{\sigma_{\ln D_i} \sigma_{\ln D_j}} = \frac{\sigma_\eta^2 + \rho_{\varepsilon_i \varepsilon_j}(\Delta_{ij}) \sigma_\varepsilon^2}{\sigma_\eta^2 + \sigma_\varepsilon^2}. \quad (2)$$

The examples in this paper adopt the attenuation relation model by [32] to predict the mean of the natural logarithm of the PGA demand at the  $i^{\text{th}}$  component as

$$\ln \bar{D}_i = -0.5265 - 0.0115 \sqrt{R_i^2 + 1.35^2} + \ln(R_i^2 + 1.35^2) [-0.3303 + 0.0599(M_w - 4.5)], \quad (3)$$

where  $M_w$  is the moment magnitude; and both  $R_i$  and  $\Delta_{ij}$  are given in km. In this paper, the standard deviations of the inter- and intra-event residuals,  $\sigma_\eta$  and  $\sigma_\varepsilon$ , are set to 0.265 and 0.502, respectively [33]. The intra-event spatial correlation is calculated by the model proposed by [31] as

$$\rho_{\varepsilon_i \varepsilon_j}(\Delta_{ij}) = \exp(-0.27 \Delta_{ij}^{0.40}). \quad (4)$$

### 2.1.2. Component failure probabilities and correlation coefficients

The seismic capacity of component  $i$ ,  $C_i$ , is modeled by a lognormal distribution with a median  $\bar{C}_i$  and lognormal standard deviation  $\zeta_i$  [33–36]. Then, the Bernoulli variable  $B_i$  representing the failure event of component  $i$ , i.e., the event when the seismic demand  $D_i$  exceeds the seismic capacity  $C_i$ , is defined as

$$B_i = \mathbb{I}(C_i \leq D_i) = \mathbb{I}(z_i \leq 0), \quad (5)$$

where  $\mathbb{I}(\cdot)$  denotes a binary indicator function that returns 1 if the given inequality holds, and 0 otherwise; and  $z_i = \ln C_i - \ln D_i$  denotes the logarithmic safety margin [37]. The seismic demand  $D_i$  and the seismic capacity  $C_i$  are assumed to be statistically independent. Since both  $D_i$  and  $C_i$  follow lognormal distributions,  $z_i$  follows a normal distribution with a mean  $\mu_{z_i} = \ln \bar{C}_i - \ln \bar{D}_i$  and a variance  $\sigma_{z_i}^2 = \zeta_i^2 + \sigma_\eta^2 + \sigma_\varepsilon^2$ . Then, the seismic failure probability of component  $i$ ,  $P_i$ , is given as

$$P_i = \mathbb{E}[B_i] = \mathbb{E}[\mathbb{I}(z_i \leq 0)] = \Phi(-\beta_i), \quad (6)$$

where  $\Phi(\cdot)$  is the standard normal cumulative distribution function (CDF); and  $\beta_i = \mu_{z_i}/\sigma_{z_i}$  denotes the reliability index.

Eq.(6) can be extended to derive the joint failure probability of components numbered from 1 to  $N$  as

$$P \left[ \bigcap_{i=1}^N \{z_i \leq 0\} \right] = \Phi_N(-\boldsymbol{\beta}, \mathbf{R}_{\mathbf{zz}}), \quad (7)$$

where  $\Phi_N(\cdot, \cdot)$  is the  $N$ -variate zero-mean, unit variance normal CDF;  $\boldsymbol{\beta} = [\beta_1, \dots, \beta_N]^T$  is the vector of reliability indices;  $\mathbf{R}_{\mathbf{zz}} = [\rho_{z_i z_j}]_{i,j \in [1, N]}$  is the  $N \times N$  correlation matrix, which is equivalent to the covariance matrix in the present context; and  $\rho_{z_i z_j}$  is the correlation coefficient between  $z_i$  and  $z_j$ . Lee and Song (2021) [36] analytically derived the correlation coefficient  $\rho_{z_i z_j}$  from Eq.(2) as

$$\rho_{z_i z_j} = \frac{\zeta_i \zeta_j \delta_{ij} + \sigma_\eta^2 + \sigma_\varepsilon^2 \rho_{\varepsilon_i \varepsilon_j}(\Delta_{ij})}{\sqrt{\zeta_i^2 + \sigma_\eta^2 + \sigma_\varepsilon^2} \sqrt{\zeta_j^2 + \sigma_\eta^2 + \sigma_\varepsilon^2}}, \quad (8)$$

where  $\delta_{ij}$  is the Kronecker delta, which is 1 when  $i = j$ , and 0 otherwise. Eq.(8) dramatically reduces the computation time of the correlation coefficients compared to numerical methods while maintaining accuracy.

If the seismic capacities do not follow the lognormal distributions as assumed in this paper, one can use the first- and second-order approximations [37] of the reliability index  $\beta_i$  and Eq.(8), i.e.,

$$\beta_i \cong \frac{\ln \mu_{C_i} - 0.5\delta_{C_i}^2 - \ln \bar{D}_i}{\sqrt{\delta_{C_i}^2 + \sigma_\eta^2 + \sigma_\varepsilon^2}}, \quad (9)$$

$$\rho_{z_i z_j} \cong \frac{\delta_{C_i} \delta_{C_j} \delta_{ij} + \sigma_\eta^2 + \sigma_\varepsilon^2 \rho_{\varepsilon_i \varepsilon_j}(\Delta_{ij})}{\sqrt{\delta_{C_i}^2 + \sigma_\eta^2 + \sigma_\varepsilon^2} \sqrt{\delta_{C_j}^2 + \sigma_\eta^2 + \sigma_\varepsilon^2}}, \quad (10)$$

where  $\mu_{C_i}$ ,  $\sigma_{C_i}$ , and  $\delta_{C_i} = \sigma_{C_i}/\mu_{C_i}$  denote the mean, standard deviation, and coefficient of variation (c.o.v.) of  $C_i$ , respectively.

## 2.2. Network reliability analysis

A lifeline network consists of line-type components, such as pipelines and roads, and node-type components, such as stations and bridges. The network can be described by a graph  $G(\mathbf{V}, \mathbf{E})$ , where  $\mathbf{V}$  denotes the set of nodes (or vertices) representing both types of components, and  $\mathbf{E}$  is the set of links (or edges) indicating the conceptual connectivity between nodes. That is, it is assumed that all links in set  $\mathbf{E}$  are perfectly reliable. This assumption will not cause error in the network reliability analysis because nodes represent the physical entities. The above assumption still holds for networks with link failures by a polynomial-time conversion to equivalent networks with node failures [38, 39].

Consider a network state vector  $\mathbf{z} = [z_1, \dots, z_N]$ , denoting a vector of the logarithmic safety margins of components, where  $N = |\mathbf{V}|$  is the number of nodes (i.e., the total number of node-type and line-type components) in the network of interest. The network reliability problem computes the network failure probability  $P_f$  by  $N$ -fold integral in the space of the network state vector, i.e.,

$$P_f = \int_{\mathcal{F}} f_{\mathbf{z}}(\mathbf{z}) d\mathbf{z} = \int_{\mathbb{R}^N} \mathbb{I}(G(\mathbf{z}) \leq 0) f_{\mathbf{z}}(\mathbf{z}) d\mathbf{z}, \quad (11)$$

where  $\mathcal{F} = \{G(\mathbf{z}) \leq 0\}$  is the failure domain for the network reliability problem, such as connectivity reliability (e.g., two-terminal reliability) and capacity reliability [40];  $G(\mathbf{z}) \in \mathbb{R}$  is the network limit-state function; and  $f_{\mathbf{z}}(\mathbf{z})$  is the joint probability density function (PDF) of the network state vector  $\mathbf{z}$ .

For the two-terminal reliability between an origin-destination (OD) node pair, the network limit-state function in Eq.(11) is defined as the binary limit-state function

$$G_{\text{OD}}^{\text{Bi}}(\mathbf{z}) = \begin{cases} 1, & \text{if the OD pair is connected in } \mathbf{z}, \\ 0, & \text{otherwise,} \end{cases} \quad (12)$$

which depends on the network topology. For example, in a series system, only the joint survival of all components guarantees connectivity. In contrast, a parallel system will fail if and only if all components fail. That is, the failure domains of  $N$ -component series and parallel systems,  $\mathcal{F}_{\text{series}}$  and  $\mathcal{F}_{\text{parallel}}$ , are defined respectively as

$$\mathcal{F}_{\text{series}} = \{G_{\text{series}}^{\text{Bi}}(\mathbf{z}) = 0\} = \bigcup_{i=1}^N \{B_i = 1\} = \left\{ \min_{i=1, \dots, N} z_i \leq 0 \right\}, \quad (13)$$

$$\mathcal{F}_{\text{parallel}} = \{G_{\text{parallel}}^{\text{Bi}}(\mathbf{z}) = 0\} = \bigcap_{i=1}^N \{B_i = 1\} = \left\{ \max_{i=1, \dots, N} z_i \leq 0 \right\}, \quad (14)$$

where  $G_{\text{series}}^{\text{Bi}}$  and  $G_{\text{parallel}}^{\text{Bi}}$  respectively denote the cases of binary network limit-state functions with series and parallel systems for an OD pair.

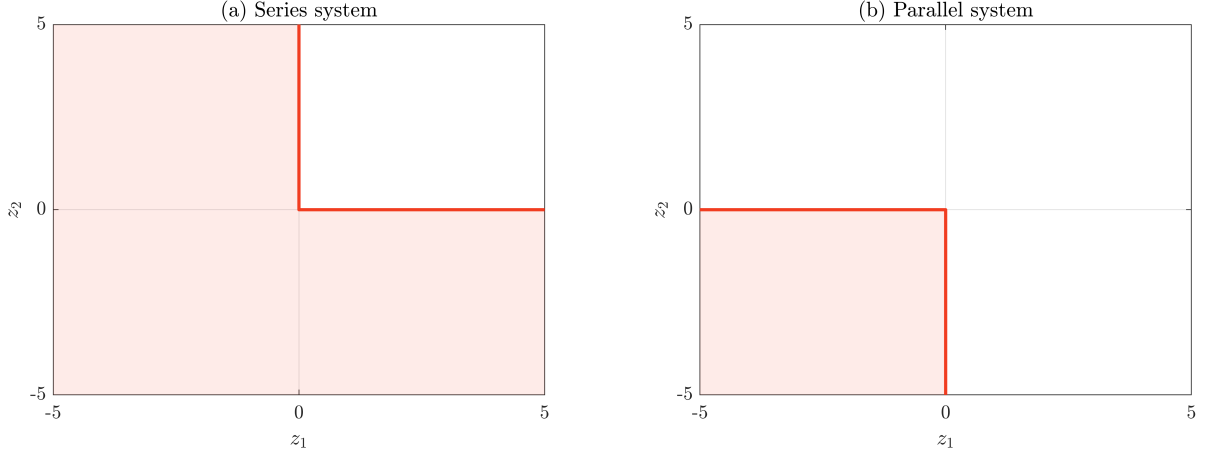


Figure 1: Failure domains of (a) two-component series system; and (b) two-component parallel system.

For example, consider two-component series and parallel systems. According to Eqs.(13) and (14), the failure domains for  $\mathcal{F}_{\text{series}}$  and  $\mathcal{F}_{\text{parallel}}$  are shown in red in Figures 1(a) and (b), respectively. The exact failure probabilities of each system  $P_f$  can be evaluated by integrating  $f(\mathbf{z})$  over each failure domain  $\mathcal{F}$ .

Series and parallel systems can be considered as networks with a link set (i.e., a set of nodes forming a single path between the OD pair) and a cut set (i.e., a set of nodes whose simultaneous failure results in the disconnection of the OD pair), respectively. In other words, by generalizing Eqs.(13) and (14), respectively, the failure domain of a general network,  $\mathcal{F}$ , is given in two ways [41] as

$$\mathcal{F} = \bigcap_{\forall k} \bigcup_{i \in L_k} \{B_i = 1\} = \left\{ \max_k \min_{i \in L_k} z_i \leq 0 \right\}, \quad (15)$$

$$\mathcal{F} = \bigcup_{\forall l} \bigcap_{i \in C_l} \{B_i = 1\} = \left\{ \min_l \max_{i \in C_l} z_i \leq 0 \right\}, \quad (16)$$

where  $L_k$  and  $C_l$  denote the  $k^{\text{th}}$  link set and the  $l^{\text{th}}$  cut set, respectively.

Once all the cut sets or link sets in a network with  $N$  components are identified, the exact network reliability can be evaluated by combining Eq.(11) with Eq.(15) or (16). To this end, several non-simulation-based methods have been developed to identify all link sets [42, 43] or cut sets [44, 45]. In addition, one can use partial link sets and cut sets to compute the upper and lower bounds of the network reliability [33, 35, 36, 46]. However, reliability problems for general networks are NP-hard [38, 47], i.e., no polynomial-time algorithm exists. Therefore, non-simulation-based approaches can be inappropriate for large-scale networks. In summary, reliability analyses of large-scale networks often face challenges in (1) exploration of the failure domain in  $2^N$  component state combinations, and (2) fast and accurate computation of probability in the high-dimensional space  $\mathbb{R}^N$ .

### 3. Subset simulation for network reliability analysis

#### 3.1. Review of subset simulation

Subset simulation (SS) [13] is one of the most widely used variance-reduction sampling approaches. In SS, the failure domain of interest,  $\mathcal{F}$ , is represented by  $m$  nested intermediate failure domains,  $\mathcal{F}_1 \supset \mathcal{F}_2 \supset \dots \supset \mathcal{F}_m = \mathcal{F}$ . The failure probability  $P_f$  is expressed as the product of the conditional probabilities  $P(\mathcal{F}_k | \mathcal{F}_{k-1})$ , i.e.,

$$P_f = \prod_{k=1}^m P(\mathcal{F}_k | \mathcal{F}_{k-1}), \quad (17)$$

where  $\mathcal{F}_0 = \mathbb{R}^N$  denotes the initial null failure domain. By setting each (except the last) conditional probability identical to a constant  $p_0$ , the intermediate failure domains  $\mathcal{F}_k$ ,  $k = 1, \dots, m-1$ , are adaptively determined by the  $p_0$  quantile of limit-state function values associated with sample points in  $\mathcal{F}_{k-1}$ . Au and Beck (2001) [13] proposed setting  $p_0 = 0.1$ , and Zuev et al. (2012) [48] demonstrated that  $p_0 \in [0.1, 0.3]$  has optimal performance.

While generating independent and identically distributed samples from the initial null failure domain is typically feasible and straightforward, it becomes challenging for the intermediate failure domains  $\mathcal{F}_{k-1}$ ,  $k \geq 2$ . To this end, Markov Chain Monte Carlo (MCMC) methods, such as the Metropolis-Hastings algorithm [49–51], can be utilized. Using an MCMC method, each conditional probability  $P(\mathcal{F}_k|\mathcal{F}_{k-1})$ , and the failure probability estimation  $\hat{P}_{f,SS}$ , can be expressed as follows, respectively:

$$P(\mathcal{F}_k|\mathcal{F}_{k-1}) = \int_{\mathcal{F}_k} f(\mathbf{z}|\mathcal{F}_{k-1}) d\mathbf{z} \cong \frac{1}{n} \sum_{j=1}^n \mathbb{I}(\mathbf{z}^{(j)} \in \mathcal{F}_k | \mathcal{F}_{k-1}), \quad (18)$$

$$\hat{P}_{f,SS} = \prod_{k=1}^m P(\mathcal{F}_k|\mathcal{F}_{k-1}) \cong \frac{p_0^{m-1}}{n} \sum_{j=1}^n \mathbb{I}(\mathbf{z}^{(j)} \in \mathcal{F} | \mathcal{F}_{m-1}), \quad (19)$$

where  $n$  is the number of sample points generated in each intermediate failure domain; and  $\mathbf{z}^{(j)}$  is the  $j^{th}$  sample point. SS is particularly efficient for rare events because the number of samples required for a single run of SS is  $n_{SS} \propto |\log P_f|$  [13], while the crude Monte Carlo simulation (MCS) requires  $n_{MCS} \propto 1/P_f$  simulations.

MCMC methods have a critical impact on the performance of SS; ideally, the MCMC sample should show limited random walk behavior and achieve rapid mixing. In this work, we adopt the Hamiltonian Monte Carlo-based subset simulation (HMC-SS) [18, 19], an efficient variant of SS leveraging the desirable properties of HMC.

### 3.2. Informative network limit-state function for subset simulation

The two-terminal reliability is typically represented by the binary limit-state function in Eq.(12). This property is a major obstacle to using SS in network reliability analysis. Provided with a binary function, the  $p_0$  quantile of the samples is chosen to be either 0 or 1 in each intermediate domain, so SS may not identify the failure domain effectively. To address this problem, the binary network limit-state function  $G_{OD}^{Bi}(\mathbf{z})$  should be reformulated as a multi-state or continuous function.

#### 3.2.1. Most reliable path-based network limit-state function

We propose an informative network limit-state function, which encodes the same failure domain as the original binary function but provides additional information on the direction and distance to the failure domain. To this end, we introduce the most reliable path (RP) concept, defined as the path between an OD pair with the highest probability of survival [33]. It follows that the network limit-state function is defined based on the vulnerability of the RP as follows:

$$G_{OD}^{RP}(\mathbf{z}) = \begin{cases} \frac{\min_{i \in \mathbf{RP}} z_i}{n_{RP}}, & \text{if the OD pair is connected in } \mathbf{z}, \\ 0, & \text{otherwise,} \end{cases} \quad (20)$$

where  $\mathbf{RP}$  denotes the set of nodes on the most reliable path with positive  $z_i$ ; and  $n_{RP}$  is the number of nodes in  $\mathbf{RP}$ . The limit-state function proposed in Eq.(20) stems from the observation that (1) the network fails if the RP fails, and (2) the larger  $n_{RP}$  is, the more likely the RP (a series system) tends to fail. Because of the denominator  $n_{RP}$ , the proposed function is piecewise rather than globally continuous; there may be a discontinuity along the boundaries where RP changes.

To find the RP, all component failure events are assumed to be independent. This independence assumption is applied only for identifying the RP. Then, Dijkstra's algorithm [52, 53] is used to find the RP

that maximizes the product of the survival probabilities of nodes obtained from Eq.(6), i.e., the sum of the log-scaled survival probabilities. Figures 2(a) and (b) visualize the proposed network limit-state functions by color maps (black: disconnection, white: robust connection) for the two-component series and parallel systems, which are contrasted with the binary functions in Figures 1(a) and (b).

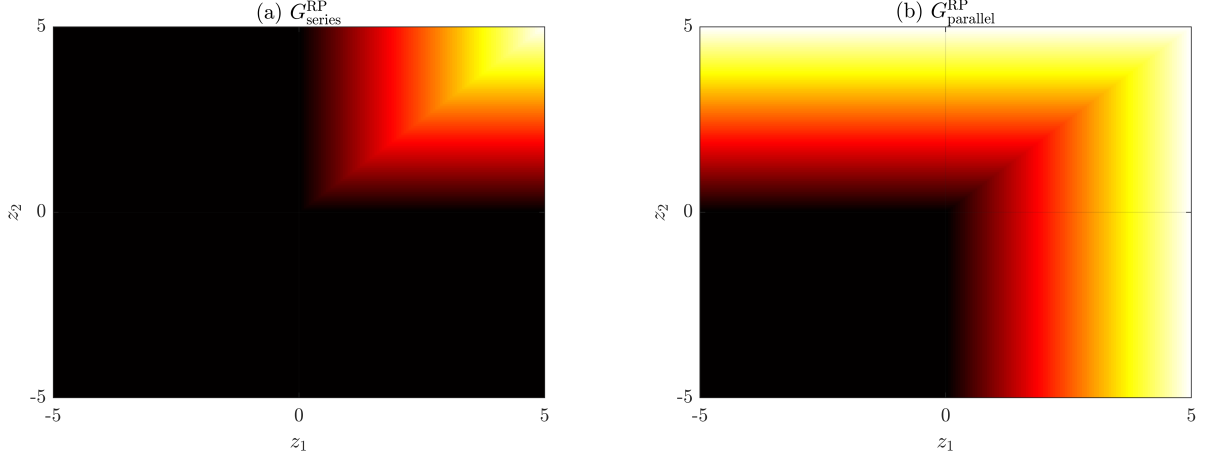


Figure 2: Proposed RP-based network limit-state function for (a) two-component series system; and (b) two-component parallel system.

Figure 2 shows that the proposed function monotonically decreases as it approaches the failure domain, so the intermediate domain gradually converges to the failure domain as SS progresses. Let the  $k^{th}$  intermediate failure domain  $\mathcal{F}_k$  be  $\{G_{OD}^{RP}(\mathbf{z}) \leq g_k\}$ . Then, according to Eq.(19), the failure probability  $P_f$  is expressed as the product of conditional probabilities as

$$\begin{aligned} \hat{P}_{f,SS} &= \prod_{k=1}^m P(G_{OD}^{RP}(\mathbf{z}) \leq g_k | G_{OD}^{RP}(\mathbf{z}) \leq g_{k-1}) \\ &\cong \frac{p_0^{m-1}}{n} \sum_{j=1}^n \mathbb{I}(G_{OD}^{RP}(\mathbf{z}^{(j)}) \leq g_m | G_{OD}^{RP}(\mathbf{z}^{(j)}) \leq g_{m-1}), \end{aligned} \quad (21)$$

where  $g_1 > \dots > g_m = 0$  denote intermediate thresholds;  $g_0 = \infty$  denotes the initial failure threshold; and  $\mathbf{z}^{(j)}$  is the state vector of the components in the  $j^{th}$  network-state sample point.

### 3.2.2. Shortest path-based network limit-state function

The proposed most reliable path-based function  $G_{OD}^{RP}(\mathbf{z})$  has a critical flaw in terms of computation time for reliability analysis of large-scale networks; the time complexity of Dijkstra's algorithm for the weighted graphs is given by  $\mathcal{O}(|V|^2)$  [54], which is quite time-consuming compared to the breadth-first search (BFS) for the OD connectivity, i.e.,  $G_{OD}^{Bi}(\mathbf{z})$ , which has a linear time  $\mathcal{O}(|E| + |V|)$ . Although SS requires fewer simulations than the crude MCS, the high computation cost per sample can offset the benefits. To compensate for this weakness, another limit-state function that utilizes the BFS is proposed as follows by replacing the RP with the shortest path (SP):

$$G_{OD}^{SP}(\mathbf{z}) = \begin{cases} \frac{\min_{i \in \mathbf{SP}} z_i}{n_{SP}}, & \text{if the OD pair is connected in } \mathbf{z}, \\ 0, & \text{otherwise,} \end{cases} \quad (22)$$

where  $\mathbf{SP}$  denotes the set of nodes on the SP consisting of nodes with positive  $z_i$ ; and  $n_{SP}$  is the number of nodes on  $\mathbf{SP}$ . Figures 3(a) and (b) visualize the proposed SP-based network limit-state function by color



maps (black: disconnection, white: robust connection) for the two-component series and parallel systems,  $G_{\text{series}}^{\text{SP}}(\mathbf{z})$  and  $G_{\text{parallel}}^{\text{SP}}(\mathbf{z})$ . Figure 3(a) for  $G_{\text{series}}^{\text{SP}}(\mathbf{z})$  is the same as Figure 2(a) for  $G_{\text{series}}^{\text{RP}}(\mathbf{z})$ , since there is only a single path in a series system, i.e.,  $\mathbf{SP} \equiv \mathbf{RP}$ . On the other hand, there is an apparent difference between the two color maps in the parallel system; in contrast to  $G_{\text{parallel}}^{\text{RP}}(\mathbf{z})$  in Figure 2(b),  $G_{\text{parallel}}^{\text{SP}}(\mathbf{z})$  has the discontinuity along the boundary between the first and second quadrants because the SP considers only the first component when both survive (i.e., the first quadrant in Figure 3(b)). This distinctively shaped network limit-state function results in a larger variance of SS estimates but requires less computation cost than the RP-based function.

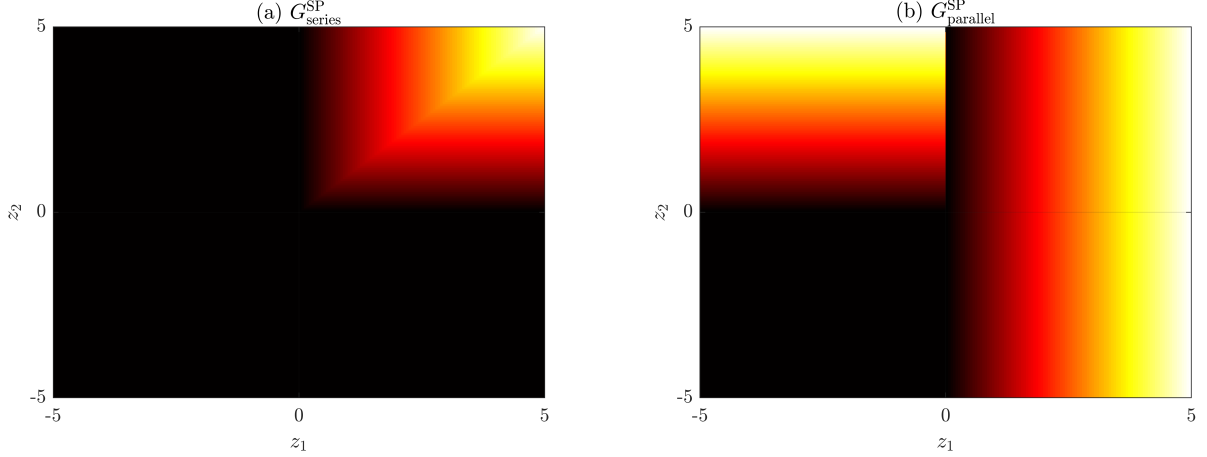


Figure 3: Proposed SP-based network limit-state function for (a) two-component series system; and (b) two-component parallel system.

### 3.2.3. Extension to $k$ -terminal reliability & $k$ -out-of- $N$ reliability

The analysis of network capacity reliability is much more complex than that of two-terminal reliability. It requires different methods tailored to the characteristics of each reliability problem (e.g., BFS for connectivity reliability, Ford-Fulkerson algorithm [55] for capacity reliability). In contrast, simulation-based analysis can be used for different network reliability problems in the same way as for the two-terminal reliability problem once their limit-state functions are well defined.

For example, we can consider  $k$ -terminal reliability [12], a generalization of two-terminal reliability. More specifically,  $k$ -terminal reliability is defined as the probability that all nodes in  $\mathbf{V}_O$  are connected to all nodes in  $\mathbf{V}_D$ , where  $\mathbf{V}_O$  and  $\mathbf{V}_D$  denote the sets of origin and destination nodes, respectively, and  $k = |\mathbf{V}_O| + |\mathbf{V}_D|$ . The network limit-state functions for two-terminal reliability are extended to the limit-state function for  $k$ -terminal reliability,  $G_k(\mathbf{z})$ , as

$$G_k(\mathbf{z}) = \min_{O_i \in \mathbf{V}_O, D_j \in \mathbf{V}_D} G_{O_i D_j}(\mathbf{z}). \quad (23)$$

Because connectivity is checked repeatedly as many times as the number of OD pairs per sample, the computational complexity of  $k$ -terminal reliability evaluation grows proportionally with  $k$ .

Furthermore, the limit-state function for  $k$ -out-of- $N$  reliability,  $G_{k/N}$ , i.e., the probability that at least  $k$  among  $N$  OD pairs are connected [56], can be formulated as

$$G_{k/N}(\mathbf{z}) = \max_{i \in [1, N]} (G_{OD_i}(\mathbf{z}), k), \quad (24)$$

where  $\max(\cdot, j)$  is defined as the function that returns the  $j^{\text{th}}$  largest value. It is noteworthy that  $G_{k/N}$  becomes identical to  $G_k$ , when  $k = N$ . In analytical methods [23, 24], the time complexity for  $k$ -out-of- $N$  reliability is given by  $\mathcal{O}(N \cdot k)$ . However, when utilizing order statistic functions like Eq.(24), the complexity remains proportional to  $N$ , independent of  $k$ .



### 3.3. Framework to assess network seismic fragility curves

On top of estimating the network failure probability for one earthquake magnitude, the proposed informative network limit-state functions also enable SS to evaluate network fragility curves. In particular, the intermediate failure domains in SS are now redefined as the failure domain under each  $M_w$ , and their probabilities correspond to discretized points on a fragility curve, with the x-axis representing the magnitude and the y-axis describing the network failure probability. To this end, this section introduces the process of configuring the intermediate failure domains and generating the network fragility curve.

#### 3.3.1. Configuration of the intermediate failure domains

Unlike individual structures, lifeline networks are distributed in a large area. Since IMs are measured differently across all sites for the same earthquake, it is considered more appropriate to use  $M_w$  as the x-axis in the network fragility curves. Consider the case where  $M_w$  changes, while the epicenter remains constant. In that case,  $\mathbf{z}$  is represented as a function of  $M_w$ , i.e.,  $\mathbf{z}(M_w)$ . While seismic demands depend on  $M_w$ , seismic capacities as well as the inter- and intra-event residuals remain unaltered regardless of  $M_w$ . In other words, as  $M_w$  varies, the covariance matrix  $\mathbf{R}_{\mathbf{z}\mathbf{z}} = [\rho_{z_i z_j}]_{N \times N}$  remains constant, and only the mean of  $\mathbf{z}(M_w)$  changes. For example, Figure 4 shows the iso-density map of  $\mathbf{z}(M_w)$  across several  $M_w$ , and the failure domains of a two-component parallel system, with more details provided in Appendix A. The failure domains are identical to those in Figure 1(b), regardless of  $M_w$ .

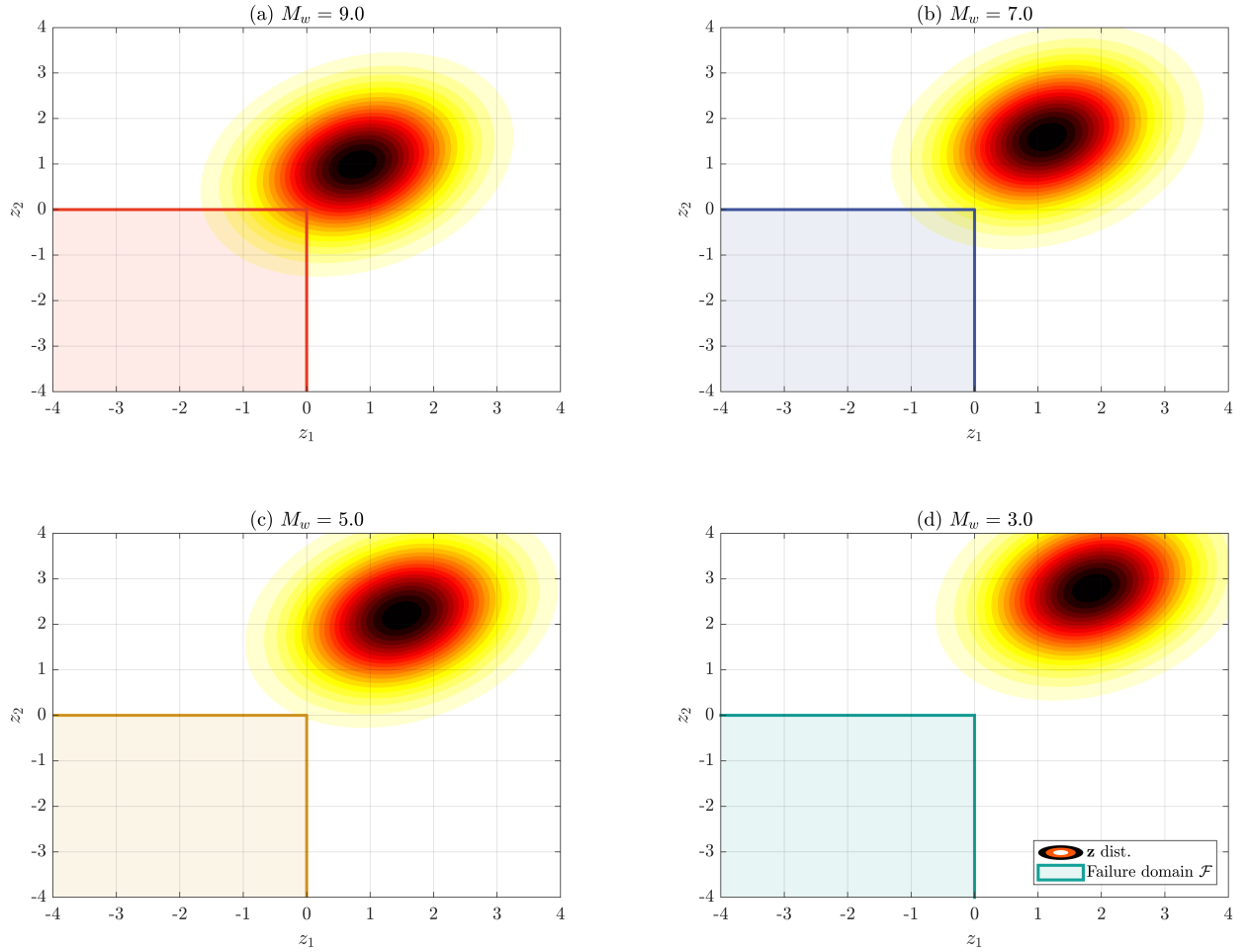


Figure 4: Failure domains of two-component parallel system and color maps of logarithmic safety margins of components under different  $M_w$ .

Let  $F_k$  be the network failure domain under an earthquake with the  $k^{th}$  moment magnitude  $M_w^k$ , where  $M_w^1 > M_w^2 > \dots > M_w^m$ . Owing to the constant  $\mathbf{R}_{\mathbf{z}\mathbf{z}}$ , all distributions of  $\mathbf{z}(M_w^k)$  can be matched to that of  $\mathbf{z}(M_w^1)$  by a linear transformation. Note that, unlike the conventional subset simulation where a relaxation parameter can be explicitly introduced to yield  $\{G(\mathbf{z}(M_w^k)) \leq g_k\}$ , the network limit-state function is nonlinear and a “ $g_k$ ” term cannot be factorized out of  $G(\cdot)$ . Therefore, we define  $F_k$  as

$$\begin{aligned} F_k &= \{G(\mathbf{z}(M_w^k)) \leq 0\} \\ &= \{G(\mathbf{z}(M_w^1) + \mathbf{z}(M_w^k) - \mathbf{z}(M_w^1)) \leq 0\} \\ &= \{G(\mathbf{z}(M_w^1) + (k-1)\Delta\mathbf{z}) \leq 0\}, \end{aligned} \quad (25)$$

where  $k = 1, 2, \dots, m$ , and  $G(\cdot)$  denotes a network limit-state function, such as  $G_{OD}$ ,  $G_k$ , and  $G_{k/N}$ . Here, we enforce a constant magnitude decrement, i.e.,  $\Delta M_w = M_w^{k+1} - M_w^k$  is set to a negative constant. In terms of Eq.(3),  $\mathbf{z}(M_w)$  is a linear function of  $M_w$ ; therefore,  $\Delta\mathbf{z} = \mathbf{z}(M_w^k) - \mathbf{z}(M_w^{k-1})$  is also a constant vector. The last line of Eq.(25) presents an interpretable form of the intermediate failure domains for a “specialized” SS for the network fragility, an extension of the conventional SS with a relaxation parameter introduced into the limit-state function. It is seen from Eq.(25) that the relaxation parameter is  $k \geq 1$ , and the effect of applying  $k > 1$  is to increase the safety margins for all network nodes. It is worth mentioning that in [20], a more general variation of SS is investigated, yielding a family of sequential sampling methods that do not rely on nested intermediate failure domains. Figure 5 illustrates the intermediate failure domains transformed from Figure 4.

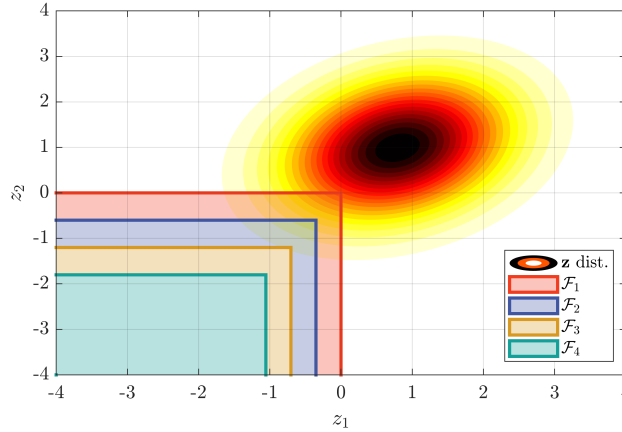


Figure 5: Overlapped color maps and intermediate failure domains by linear transformation.

### 3.3.2. Generation of network fragility curves

Using Eq.(25), a single implementation of the specialized SS can yield the network failure probabilities at multiple values of  $M_w$ , i.e., the fragility curve. This practice requires significantly fewer samples than the crude MCS or repeatedly applying SS for each  $M_w$ . If a conditional probability  $P(\mathcal{F}_i|\mathcal{F}_{i-1})$  for a pre-specified magnitude decrement is too small, similar to the conventional SS, we can adaptively reduce the decrement of  $M_w$  so that the conditional probability becomes large, i.e., building an adaptive mesh refinement for the fragility curve.

## 4. Numerical examples

Three numerical examples are considered to demonstrate the efficiency and accuracy of the proposed network limit-state functions and the method for network fragility curve evaluation: (1) two-terminal reliability on the two-component parallel system, (2)  $k$ -terminal reliability on the San Jose highway bridge network [12, 36, 57], and (3)  $k$ -out-of- $N$  reliability on the San Diego highway bridge network [36]. In each of these examples, the

seismic capacity parameters for the components or bridges are fixed at 0.98 for the median  $\bar{C}_i$ , and 0.69 for the log-standard deviation  $\zeta_i$ . To compare the two proposed network limit-state functions,  $G_{\text{OD}}^{\text{RP}}$  and  $G_{\text{OD}}^{\text{SP}}$ , the parameters for HMC-SS are set to  $n = 1,000$ ,  $p_0 = 0.1$ ,  $t_f = \pi/4$ , and  $\alpha = 0$  (for details on the last two parameters, see [18]). All computations in this section are performed using MATLAB® on an 8-core MacBook Air (2022) with 8 GB of RAM.

#### 4.1. Example 1: a two-component parallel system

Consider the two-terminal reliability of the two-component parallel system mentioned above. For an earthquake with  $M_w = 5.0$ , Figures 6 and 7 represent the 500 HMC samples and the adaptively identified intermediate failure domains using  $G_{\text{OD}}^{\text{RP}}$  and  $G_{\text{OD}}^{\text{SP}}$ , respectively. The contour plot of the joint PDF  $f(\mathbf{z})$  and the system failure domain  $\mathcal{F}$  are also shown. In contrast to the square intermediate domains of  $G_{\text{OD}}^{\text{RP}}$ , those of  $G_{\text{OD}}^{\text{SP}}$  resemble the plots in Figure 3(b).

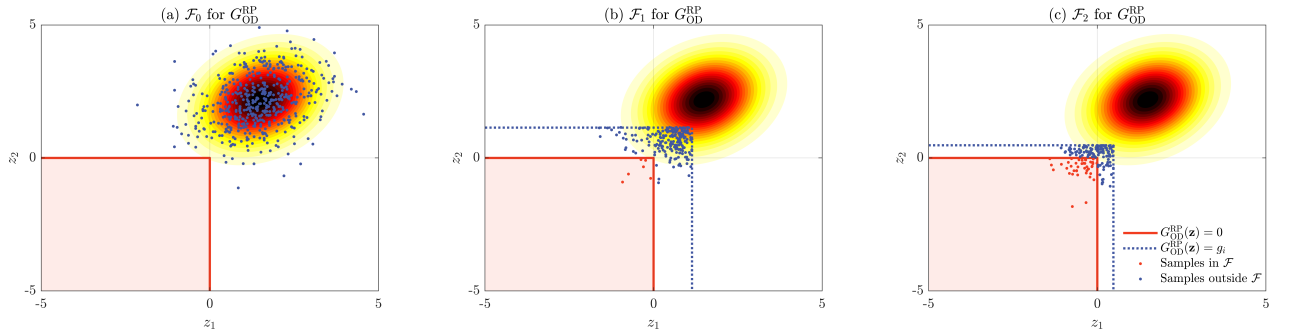


Figure 6: Samples obtained from the (a) entire domain; (b) first subset; and (c) second subset using  $G_{\text{OD}}^{\text{RP}}$ .

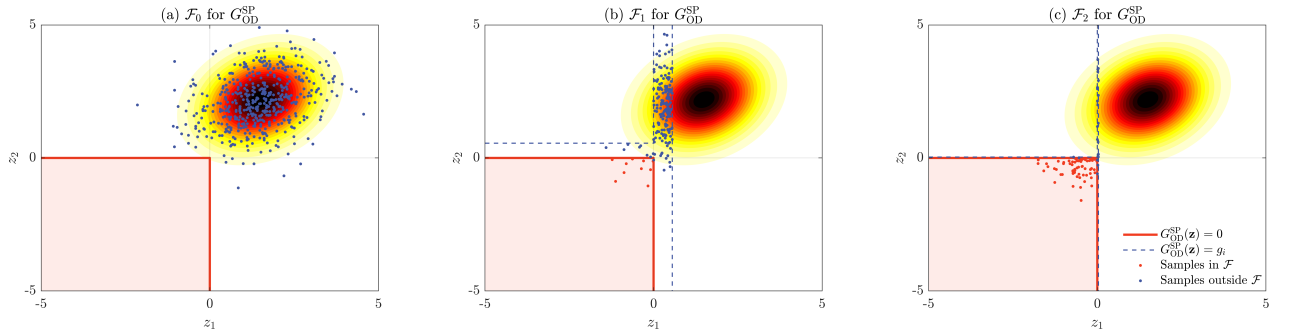


Figure 7: Samples obtained from the (a) entire domain; (b) first subset; and (c) second subset using  $G_{\text{OD}}^{\text{SP}}$ .

Table 1: Two-terminal reliability analysis results for the two-component parallel system.

$M_w$	$G_{\text{OD}}^{\text{RP}}$				$G_{\text{OD}}^{\text{SP}}$				Exact $P_f$
	$\hat{P}_{f,SS}$	c.o.v.	$N_G$	$t_{ss}(\text{s})$	$\hat{P}_{f,SS}$	c.o.v.	$N_G$	$t_{ss}(\text{s})$	
7.0	$1.41 \times 10^{-2}$	0.149	1,927	0.447	$1.41 \times 10^{-2}$	0.202	1,956	0.102	$1.40 \times 10^{-2}$
6.0	$6.34 \times 10^{-3}$	0.196	2,791	0.730	$6.37 \times 10^{-3}$	0.265	2,769	0.169	$6.30 \times 10^{-3}$
5.0	$2.62 \times 10^{-3}$	0.196	2,800	0.635	$2.63 \times 10^{-3}$	0.345	2,807	0.136	$2.61 \times 10^{-3}$
4.0	$1.00 \times 10^{-3}$	0.255	3,290	0.817	$1.00 \times 10^{-3}$	0.478	3,351	0.176	$0.98 \times 10^{-3}$
3.0	$3.46 \times 10^{-4}$	0.286	3,700	0.837	$3.50 \times 10^{-4}$	0.702	4,044	0.212	$3.40 \times 10^{-4}$

To evaluate the bias and variation of the results by the method, HMC-SS is executed 500 times using  $G_{OD}^{RP}$  and  $G_{OD}^{SP}$ . Table 1 shows the results compared with the reference  $P_f$ . The “exact”  $P_f$  of the two-component system is estimated using a two-fold numerical integration, which is infeasible for large-scale networks. While the estimates of HMC-SS are asymptotically unbiased, the solutions achieve high accuracy when compared with the reference. Table 1 summarizes the average number of network limit-state function evaluations,  $N_G$  and the computation time per run of HMC-SS,  $t_{ss}$ . We introduce  $eff = c.o.v. \times \sqrt{N_G}$  to measure the efficiency of the sampling methods [13]. Lower  $eff$  indicates high efficiency.

Figures 8(a) and 8(b) compare the efficiency of the proposed network limit-state functions in terms of  $eff$  and the computation time while varying  $M_w$ .  $G_{OD}^{RP}$ -based HMC-SS is more accurate owing to low  $c.o.v.$  of the estimated probabilities, whereas  $G_{OD}^{SP}$ -based HMC-SS takes a much shorter time. The speedup comes from the efficient shortest path search using BFS, which is considerably faster than the Dijkstra algorithm. In general, regardless of the limit-state function, as  $M_w$  decreases, the network failure probabilities decrease, and  $N_G$  and  $t_{ss}$  increase. On the other hand, there is a temporary  $t_{ss}$  inconsistency in  $4.0 < M_w < 7.0$ . This is because the time required to remove seismically damaged components in each network sample is proportional to  $M_w$ , while  $N_G$  increases. Nevertheless,  $N_G$  is the dominant factor driving the overall trend because its variation is much larger than that of the component failure probabilities.

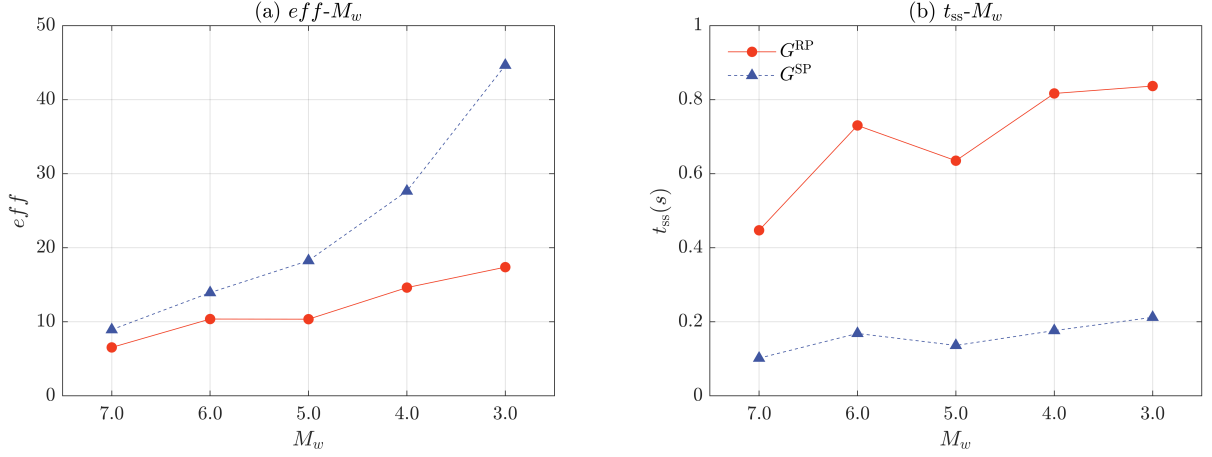


Figure 8: (a)  $eff$ ; and (b)  $t_{ss}$  according to  $M_w$  on two-component parallel system.

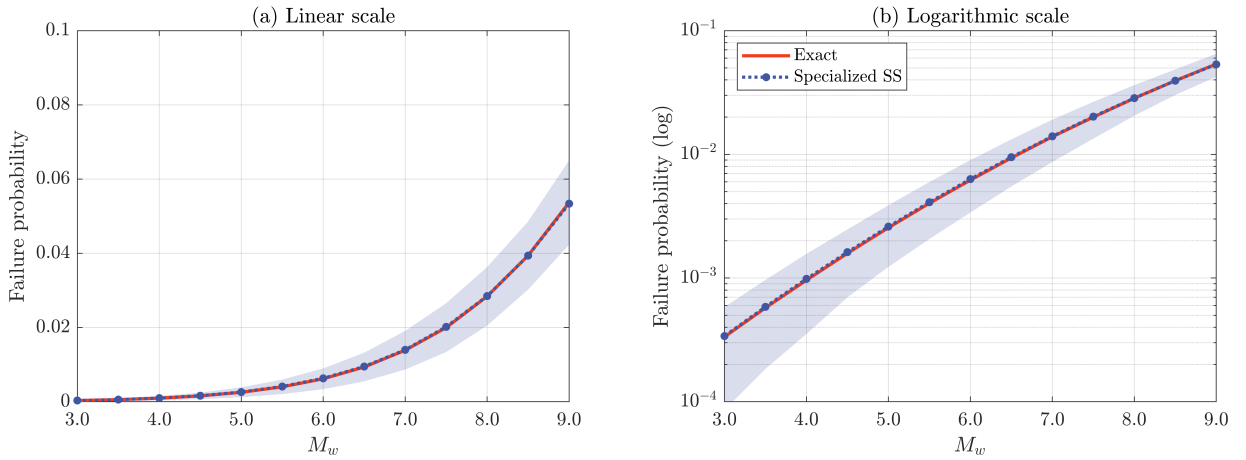


Figure 9: Seismic system fragility curves obtained by a single implementation of specialized HMC-SS.

Next, we evaluate the seismic fragility curve using the framework proposed in Section 3.3. In a single implementation of the specialized HMC-SS,  $G_{OD}^{RP}$  is adopted for its high accuracy, even though it takes longer computation time than using  $G_{OD}^{SP}$ . The range of  $M_w$  is set to  $3.0 \leq M_w \leq 9.0$  with  $\Delta M_w = 0.5$ , and the specialized HMC-SS is repeated 250 times to produce an estimate of the confidence interval. Figure 9 shows the generated seismic fragility curve (blue dashed line) along with the 95% confidence interval (blue shaded area) compared to the exact values (red solid line). The specialized HMC-SS estimates the fragility curve accurately using 12,700 limit-state function evaluations, which is only 37.47% of those required in a repeated simulation of HMC-SS for each  $M_w$ . Appendix B.1 provides the detailed results of the “one-shot” HMC-SS compared to those from separate runs.

#### 4.2. Example 2: San Jose highway bridge network

Figure 10 shows the highway bridge network in San Jose, California [36] (modified from [12, 57]) with two origins and two destinations. To analyze the  $k$ -terminal reliability (in this example,  $k = |\mathbf{V}_O| + |\mathbf{V}_D| = 4$ ), the HMC-SS using  $G_{OD}^{RP}$  and  $G_{OD}^{SP}$  are conducted 500 times, and Table 2 summarizes the performance. The reference MCS solution is obtained through crude MCS with a target  $c.o.v. = 0.01$ . The results confirm the accuracy of the HMC-SS using the proposed network limit-state functions. Figure 11 compares  $eff$  and  $t_{ss}$  obtained from the two proposed limit-state functions. Similar to Example 1, the trade-off between accuracy and efficiency seems inevitable.

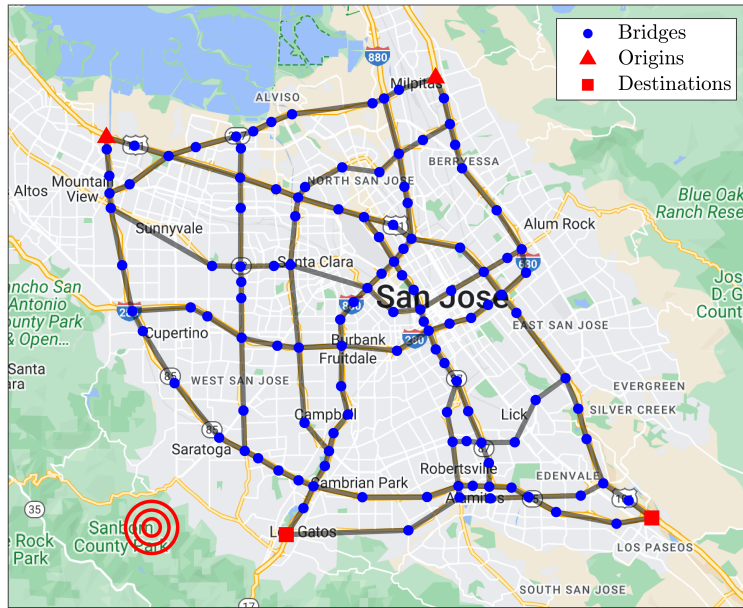


Figure 10: Highway bridge network in San Jose, CA [36].

Table 2: Four-terminal reliability analysis results on the San Jose highway bridge network.

$M_w$	$G_{OD}^{RP}$				$G_{OD}^{SP}$				MCS $P_f$
	$\hat{P}_{f,SS}$	$c.o.v.$	$N_G$	$t_{ss}(s)$	$\hat{P}_{f,SS}$	$c.o.v.$	$N_G$	$t_{ss}(s)$	
7.0	$1.54 \times 10^{-1}$	0.072	1,000	0.824	$1.53 \times 10^{-1}$	0.070	1,000	0.491	$1.54 \times 10^{-1}$
6.0	$7.17 \times 10^{-2}$	0.106	1,900	1.403	$7.19 \times 10^{-2}$	0.110	1,900	0.780	$7.25 \times 10^{-2}$
5.0	$3.35 \times 10^{-2}$	0.128	1,900	1.038	$3.32 \times 10^{-2}$	0.145	1,900	0.448	$3.32 \times 10^{-2}$
4.0	$1.60 \times 10^{-2}$	0.155	1,902	0.837	$1.57 \times 10^{-2}$	0.190	1,918	0.290	$1.56 \times 10^{-2}$
3.0	$7.54 \times 10^{-3}$	0.182	2,753	1.171	$7.68 \times 10^{-3}$	0.239	2,708	0.365	$7.56 \times 10^{-3}$

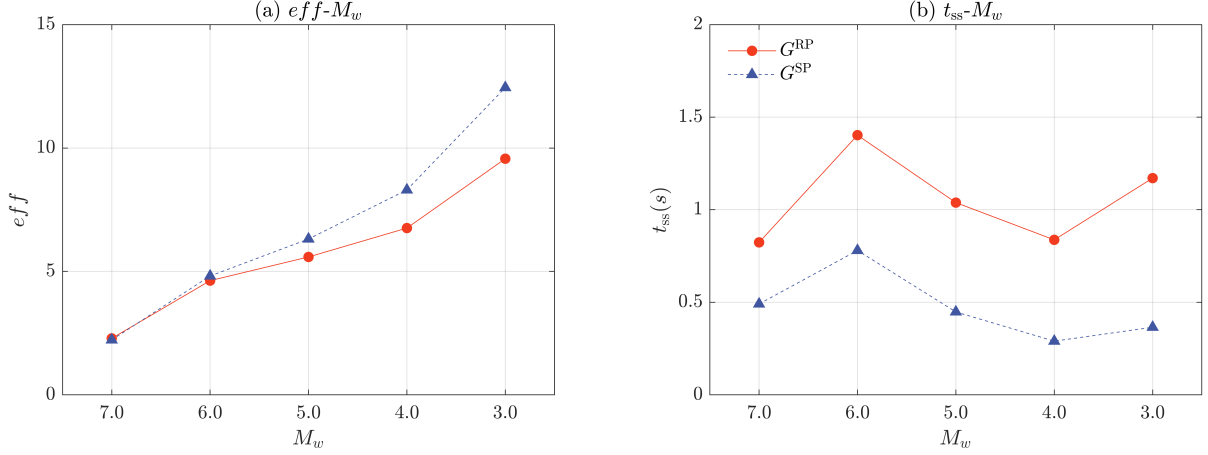


Figure 11: (a)  $eff$ - $M_w$ ; and (b)  $t_{ss}$ - $M_w$  curves on San Jose highway bridge network.

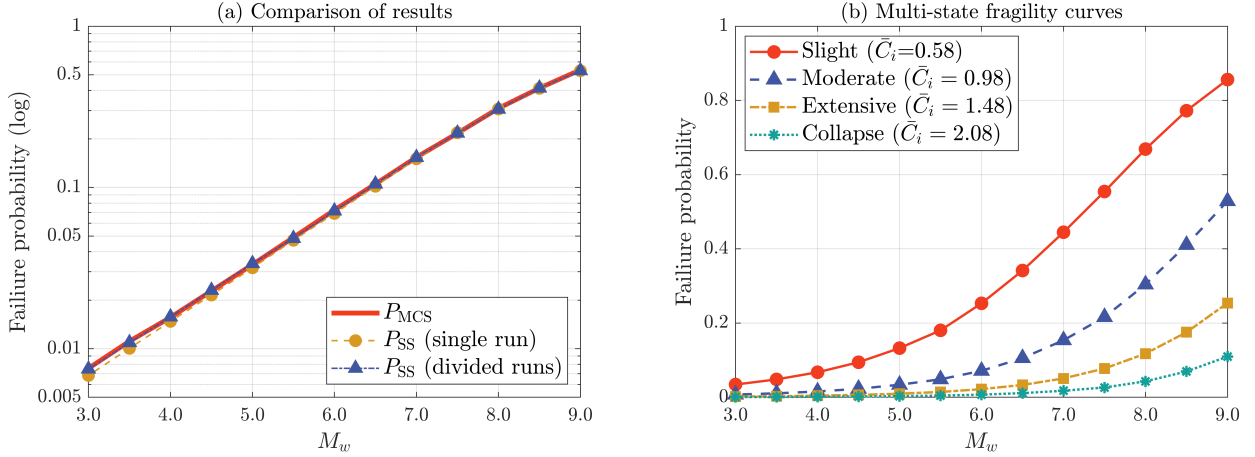


Figure 12: (a) Comparison of generated seismic fragility curves of the San Jose highway bridge network; and (b) multi-state network fragility curves obtained by specialized HMC-SS.

By substituting Eq.(23) into Eq.(25), the network fragility curve can be evaluated in terms of four-terminal reliability against the magnitude. Accumulated biases/errors of sequential conditioning are particularly conspicuous when assessing  $k$ -terminal or  $k$ -out-of- $N$  reliability in large-scale networks because of the complexity of failure domains. To minimize the error of specialized subset simulations due to accumulated bias, we divide the target range of  $M_w$  into multiple intervals, where independent specialized SSs are performed for each interval. Each run adaptively selects the intermediate failure domain using the  $p_0(=0.1)$ -quantile until the samples reach the first failure domain of the interval. This approach can be understood as using a coarse adaptive mesh controlled by  $p_0$  to reach the target interval and a uniform fine mesh controlled by  $\Delta M_w$  to generate a smooth fragility curve within the target interval. Compared with a “one-shot” run with a constant  $\Delta M_w$  to produce the entire fragility curve, this “divide-and-conquer” trick requires fewer steps to reach each interval; thus, the bias is smaller, with the cost of using more sample points. The range of  $3.0 \leq M_w \leq 9.0$  is divided into three intervals:  $3.0 \leq M_w \leq 5.0$ ,  $5.0 < M_w \leq 7.0$ , and  $7.0 < M_w \leq 9.0$ , with  $\Delta M_w = 0.5$ . In this example, HMC-SS is executed 250 times. Figure 12(a) compares the results of the crude MCS, the single implementation of the specialized HMC-SS, and three divided implementations of the specialized HMC-SS. Note that the divided run provides more accurate results consistent with the crude MCS result, while the single run underestimates the failure probabilities

when  $M_w \leq 5.0$  due to accumulation of biases/errors. To achieve better accuracy, the divided runs require only 9.32% more samples than the single run. The detailed results of the specialized HMC-SS are presented in Appendix B.2. In addition, the proposed framework can generate multi-state fragility curves, as shown in Figure 12(b). All bridges in the network are assumed to have the following median seismic capacities  $\bar{C}_i$  for each damage state: 0.58 for slight damage, 0.98 for moderate damage, 1.48 for extensive damage, and 2.08 for collapse damage. For each damage state, the log-standard deviation  $\zeta_i$  is set to 0.69.

#### 4.3. Example 3: San Diego highway bridge network

Figure 13 shows the highway bridge network in San Diego, California [36] with one origin and five destinations, connecting the southwest coast of San Diego to five nearby cities. Eq.(24) is used to evaluate the probability of at least  $k \leq 5$  destinations being accessible from the origin (i.e., the  $k$ -out-of-5 reliability). Table 3 provides a comparison of the 3-out-of-5 reliability results estimated from HMC-SS using  $G_{OD}^{RP}$  and  $G_{OD}^{SP}$ , and from the crude MCS. Additionally, Figure 14 visualizes the  $eff-M_w$  and  $t_{ss}-M_w$  curves. Similar to the previous examples, the accuracy of the proposed limit-state functions is confirmed, and the trade-off between accuracy and efficiency is observed.

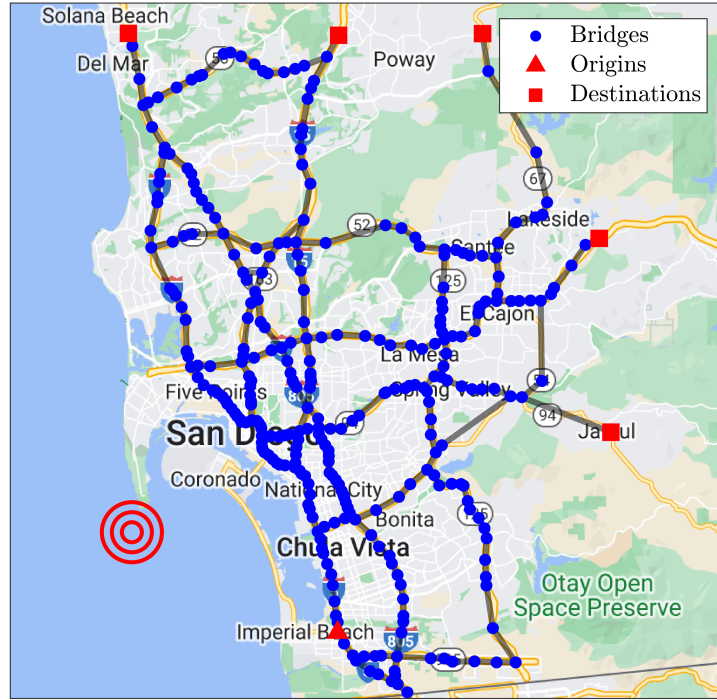


Figure 13: Highway bridge network in San Jose, CA [36].

Table 3: 3-out-of-5 reliability analysis results on the San Diego highway bridge network.

$M_w$	$G_{OD}^{RP}$				$G_{OD}^{SP}$				MCS $P_f$
	$\hat{P}_{f,SS}$	$c.o.v.$	$N_G$	$t_{ss}(s)$	$\hat{P}_{f,SS}$	$c.o.v.$	$N_G$	$t_{ss}(s)$	
7.0	$1.19 \times 10^{-1}$	0.088	1,032	0.590	$1.19 \times 10^{-1}$	0.082	1,025	0.421	$1.17 \times 10^{-1}$
6.0	$3.42 \times 10^{-2}$	0.129	1,900	2.233	$3.39 \times 10^{-2}$	0.131	1,900	1.674	$3.38 \times 10^{-2}$
5.0	$8.03 \times 10^{-3}$	0.192	2,697	2.932	$8.03 \times 10^{-3}$	0.228	2,676	1.911	$8.07 \times 10^{-3}$
4.0	$1.76 \times 10^{-3}$	0.274	2,823	2.356	$1.76 \times 10^{-3}$	0.359	2,894	1.205	$1.69 \times 10^{-3}$
3.0	$3.57 \times 10^{-4}$	0.333	3,700	2.891	$3.73 \times 10^{-4}$	0.600	3,777	1.218	$3.62 \times 10^{-4}$



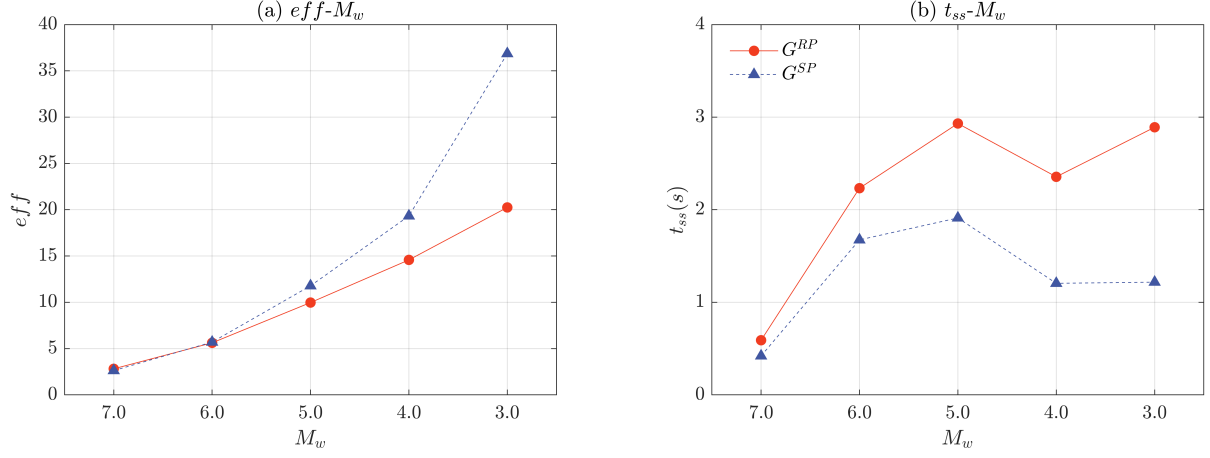


Figure 14: (a)  $eff-M_w$ , and (b)  $t_{ss}-M_w$  curves on San Diego highway bridge network.

For fragility analysis, the range of  $3.0 \leq M_w \leq 9.0$  is divided into two intervals, i.e.,  $3.0 \leq M_w \leq 6.0$ , and  $6.0 < M_w \leq 9.0$ , with  $\Delta M_w = 0.5$ , and HMC-SS is repeated 250 times. Figure 15(a) shows the results of the 3-out-of-5 reliability evaluated by HMC-SS with and without division, in comparison to those by the crude MCS. As in Example 2, one can observe that the divided implementations of the HMC-SS can avoid underestimating the failure probability at low  $M_w$ , unlike the single implementation. The detailed results of the 3-out-of-5 reliability evaluated by the specialized HMC-SS are provided in Appendix B.3. By repeating this assessment process for  $1 \leq k \leq 5$ , the fragility curves are shown in Figure 15(b), where we increase the value of  $n$  to 10,000 to achieve more stable convergence.

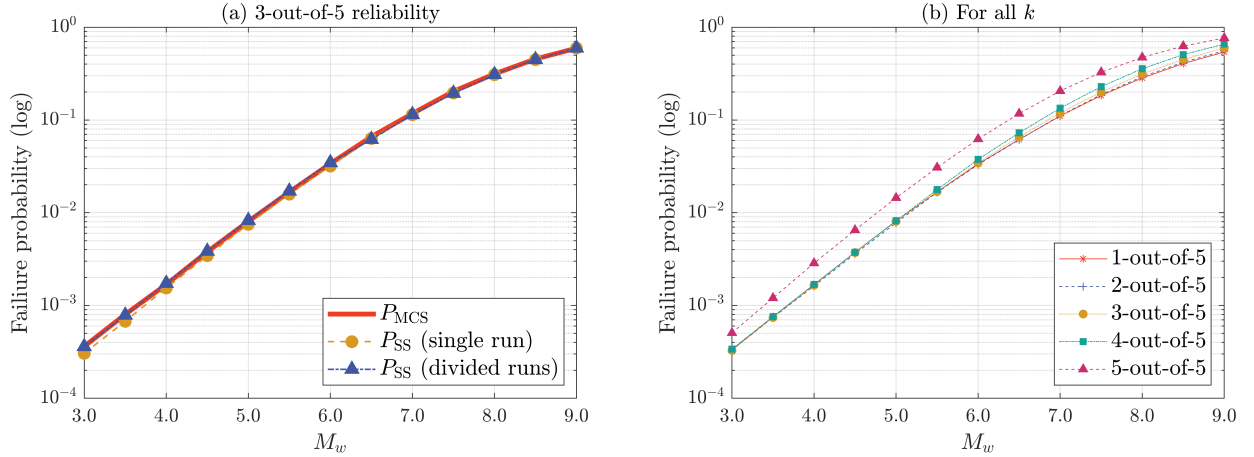


Figure 15: Seismic fragility curves of the San Diego highway bridge network for (a)  $k = 3$ ; and (b)  $1 \leq k \leq 5$ .

## 5. Conclusions

Two informative limit-state functions were proposed to reformulate the traditional binary limit-state function for two-terminal reliability analysis of lifeline networks, thereby making the application of subset simulation (SS) possible. The first limit-state function quantifies the vulnerability of the most reliable path between the origin and destination nodes, whereas the other utilizes the shortest path. Both limit-state function reformulations represent the same failure domain as the original binary limit-state function, while their function values at the safe domain differ. Moreover, a specialized SS can be developed to generate network-level fragility curves by connecting intermediate failure events to the earthquake magnitude. As a result, the

specialized SS can generate the network fragility curve in a single run. Furthermore, the sampling framework was successfully extended to assess  $k$ -terminal or  $k$ -out-of- $N$  reliability.

The accuracy and efficiency of the proposed framework were tested and demonstrated by three numerical examples using the Hamiltonian Monte Carlo-based SS. The results confirm the accuracy and efficiency of the proposed network limit-state functions. The first limit-state function generally has higher accuracy, while the second requires lower computation time.

As demonstrated by numerical examples, the proposed framework is highly scalable and can be applied to seismic fragility curves for various network reliability indices. Future research could develop informative limit-state functions tailored to each network reliability index instead of relying solely on the proposed functions that measure the vulnerability of the most reliable or shortest paths. A remaining task is to use the proposed framework to identify more realistic network reliability, such as network flow capacity. Possible solutions to this problem could involve modeling components as multi-state or continuous, or considering the flow capacity of each origin-destination pair in the proposed  $k$ -out-of- $N$  reliability analysis. Finally, probabilistic inferences, like sensitivity analysis or importance measures for each component, can be conducted.

## Acknowledgment

This work is supported by the Korea Agency for Infrastructure Technology Advancement (KAIA) grant funded by the Ministry of Land, Infrastructure and Transport (Grant RS-2021-KA163162). The corresponding author is also supported by the Institute of Construction and Environmental Engineering at Seoul National University. These supports are gratefully acknowledged.

## References

- [1] Anthony Chen, Hai Yang, Hong K Lo, and Wilson H Tang. Capacity reliability of a road network: an assessment methodology and numerical results. *Transportation Research Part B: Methodological*, 36(3):225–252, 2002.
- [2] Yi-Kuei Lin and John Yuan. Flow reliability of a probabilistic capacitated-flow network in multiple node pairs case. *Computers & industrial engineering*, 45(3):417–428, 2003.
- [3] Jianye Ching and Wei-Chih Hsu. An efficient method for evaluating origin-destination connectivity reliability of real-world lifeline networks. *Computer-Aided Civil and Infrastructure Engineering*, 22(8):584–596, 2007.
- [4] Simona Esposito, Iunio Iervolino, Anna d’Onofrio, Antonio Santo, Francesco Cavalieri, and Paolo Franchin. Simulation-based seismic risk assessment of gas distribution networks. *Computer-Aided Civil and Infrastructure Engineering*, 30(7):508–523, 2015.
- [5] Yasuo Asakura and Masuo Kashiwadani. Road network reliability caused by daily fluctuation of traffic flow. In *PTRC Summer Annual Meeting, 19th, 1991, University of Sussex, United Kingdom*, 1991.
- [6] Michael GH Bell, Chris Cassir, Yasunori Iida, and William HK Lam. A sensitivity based approach to network reliability assessment. In *14th International Symposium on Transportation and Traffic Theory* Transportation Research Institute, 1999.
- [7] Mengdie Chen, Sujith Mangalathu, and Jong-Su Jeon. Bridge fragilities to network fragilities in seismic scenarios: An integrated approach. *Engineering Structures*, 237:112212, 2021.
- [8] Xiaohang Liu, Shansuo Zheng, Xinxia Wu, Dianxin Chen, and Jinchuan He. Research on a seismic connectivity reliability model of power systems based on the quasi-monte carlo method. *Reliability Engineering & System Safety*, 215:107888, 2021.
- [9] Benwei Hou, Qianyi Xu, Zilan Zhong, Junyan Han, Huiquan Miao, and Xiuli Du. Seismic reliability evaluation of spatially correlated pipeline networks by quasi-monte carlo simulation. *Structure and Infrastructure Engineering*, pages 1–16, 2022.
- [10] Claudio M Rocco and JA Moreno. Fast monte carlo reliability evaluation using support vector machine. *Reliability Engineering & System Safety*, 76(3):237–243, 2002.
- [11] Raphael E Stern, Junho Song, and Daniel B Work. Accelerated monte carlo system reliability analysis through machine-learning-based surrogate models of network connectivity. *Reliability Engineering & System Safety*, 164:1–9, 2017.
- [12] Mohammad Amin Nabian and Hadi Meidani. Deep learning for accelerated seismic reliability analysis of transportation networks. *Computer-Aided Civil and Infrastructure Engineering*, 33(6):443–458, 2018.
- [13] Siu-Kui Au and James L Beck. Estimation of small failure probabilities in high dimensions by subset simulation. *Probabilistic Engineering Mechanics*, 16(4):263–277, 2001.
- [14] Nolan Kurtz and Junho Song. Cross-entropy-based adaptive importance sampling using gaussian mixture. *Structural Safety*, 42:35–44, 2013.
- [15] Ziqi Wang and Junho Song. Cross-entropy-based adaptive importance sampling using von mises-fisher mixture for high dimensional reliability analysis. *Structural Safety*, 59:42–52, 2016.

- [16] David Y Yang, Jin-Guang Teng, and Dan M Frangopol. Cross-entropy-based adaptive importance sampling for time-dependent reliability analysis of deteriorating structures. *Structural Safety*, 66:38–50, 2017.
- [17] Sebastian Geyer, Iason Papaioannou, and Daniel Straub. Cross entropy-based importance sampling using gaussian densities revisited. *Structural Safety*, 76:15–27, 2019.
- [18] Ziqi Wang, Marco Broccardo, and Junho Song. Hamiltonian monte carlo methods for subset simulation in reliability analysis. *Structural Safety*, 76:51–67, 2019.
- [19] Weiming Chen, Ziqi Wang, Marco Broccardo, and Junho Song. Riemannian manifold hamiltonian monte carlo based subset simulation for reliability analysis in non-gaussian space. *Structural Safety*, 94:102134, 2022.
- [20] Jianhua Xian and Ziqi Wang. Relaxation-based importance sampling for structural reliability analysis. *Structural Safety*, 106:102393, 2024.
- [21] Jianpeng Chan, Iason Papaioannou, and Daniel Straub. An adaptive subset simulation algorithm for system reliability analysis with discontinuous limit states. *Reliability Engineering & System Safety*, 225:108607, 2022.
- [22] Iason Papaioannou, Costas Papadimitriou, and Daniel Straub. Sequential importance sampling for structural reliability analysis. *Structural safety*, 62:66–75, 2016.
- [23] Richard E Barlow and Klaus D Heidtmann. Computing k-out-of-n system reliability. *IEEE Transactions on Reliability*, 33(4):322–323, 1984.
- [24] Jer-Shyan Wu and Rong-Jaye Chen. An algorithm for computing the reliability of weighted-k-out-of-n systems. *IEEE Transactions on Reliability*, 43(2):327–328, 1994.
- [25] Jack W Baker and C Allin Cornell. A vector-valued ground motion intensity measure consisting of spectral acceleration and epsilon. *Earthquake Engineering & Structural Dynamics*, 34(10):1193–1217, 2005.
- [26] Nicolas Luco and C Allin Cornell. Structure-specific scalar intensity measures for near-source and ordinary earthquake ground motions. *Earthquake Spectra*, 23(2):357–392, 2007.
- [27] Anil K Chopra. *Dynamics of Structures: Theory and Applications to Earthquake Engineering*. Prentice Hall, 1995.
- [28] Nolan Kurtz, Junho Song, and Paolo Gardoni. Seismic reliability analysis of deteriorating representative us west coast bridge transportation networks. *Journal of Structural Engineering*, 142(8):C4015010, 2016.
- [29] Norman A Abrahamson and Robert R Youngs. A stable algorithm for regression analyses using the random effects model. *Bulletin of the Seismological Society of America*, 82(1):505–510, 1992.
- [30] William B Joyner and David M Boore. Methods for regression analysis of strong-motion data. *Bulletin of the Seismological Society of America*, 83(2):469–487, 1993.
- [31] Katsuchihiro Goda and Han-Ping Hong. Spatial correlation of peak ground motions and response spectra. *Bulletin of the Seismological Society of America*, 98(1):354–365, 2008.
- [32] David M Boore and Gail M Atkinson. Ground-motion prediction equations for the average horizontal component of pga, pgv, and 5%-damped psa at spectral periods between 0.01 s and 10.0 s. *Earthquake Spectra*, 24(1):99–138, 2008.
- [33] Hyun-Woo Lim and Junho Song. Efficient risk assessment of lifeline networks under spatially correlated ground motions using selective recursive decomposition algorithm. *Earthquake Engineering & Structural Dynamics*, 41(13):1861–1882, 2012.
- [34] Bryant G Nielson and Reginald DesRoches. Seismic fragility methodology for highway bridges. In *Structures Congress 2006: Structural Engineering and Public Safety*, pages 1–9, 2006.
- [35] Hyun-Woo Lim, Junho Song, and Nolan Kurtz. Seismic reliability assessment of lifeline networks using clustering-based multi-scale approach. *Earthquake Engineering & Structural Dynamics*, 44(3):355–369, 2015.
- [36] Dongkyu Lee and Junho Song. Multi-scale seismic reliability assessment of networks by centrality-based selective recursive decomposition algorithm. *Earthquake Engineering & Structural Dynamics*, 50(8):2174–2194, 2021.
- [37] Armen Der Kiureghian. *Structural and system reliability*. Cambridge University Press, 2022.
- [38] Charles J Colbourn. Network resilience. *SIAM Journal on Algebraic Discrete Methods*, 8(3):404–409, 1987.
- [39] Michael O Ball, Charles J Colbourn, and J Scott Provan. Network reliability. *Handbooks in operations research and management science*, 7:673–762, 1995.
- [40] Konstantin M Zuev, Stephen Wu, and James L Beck. General network reliability problem and its efficient solution by subset simulation. *Probabilistic Engineering Mechanics*, 40:25–35, 2015.
- [41] Junho Song and Armen Der Kiureghian. Bounds on system reliability by linear programming. *Journal of Engineering Mechanics*, 129(6):627–636, 2003.
- [42] Jacob A Abraham. An improved algorithm for network reliability. *IEEE Transactions on Reliability*, 28(1):58–61, 1979.
- [43] MA Aziz, MA Sobhan, and MA Samad. Enumeration of pathsets of reliability graphs by repeated indexing. *Microelectronics Reliability*, 33(4):481–487, 1993.
- [44] David B Brown. A computerized algorithm for determining the reliability of redundant configurations. *IEEE Transactions on Reliability*, 20(3):121–124, 1971.
- [45] Arnie Rosenthal. Approaches to comparing cut-set enumeration algorithms. *IEEE Transactions on Reliability*, 28(1):62–65, 1979.
- [46] Jie Li and Jun He. A recursive decomposition algorithm for network seismic reliability evaluation. *Earthquake Engineering & Structural Dynamics*, 31(8):1525–1539, 2002.
- [47] Arnie Rosenthal. Computing the reliability of complex networks. *SIAM Journal on Applied Mathematics*, 32(2):384–393, 1977.
- [48] Konstantin M Zuev, James L Beck, Siu-Kui Au, and Lambros S Katafygiotis. Bayesian post-processor and other enhancements of subset simulation for estimating failure probabilities in high dimensions. *Computers & structures*, 92:283–296, 2012.
- [49] Nicholas Metropolis, Arianna W Rosenbluth, Marshall N Rosenbluth, Augusta H Teller, and Edward Teller. Equation of

- state calculations by fast computing machines. *The journal of chemical physics*, 21(6):1087–1092, 1953.
- [50] W. Keith Hastings. Monte carlo sampling methods using markov chains and their applications. *Biometrika*, pages 97–109, 1970.
- [51] Iason Papaioannou, Wolfgang Betz, Kilian Zwirgmaier, and Daniel Straub. Mcmc algorithms for subset simulation. *Probabilistic Engineering Mechanics*, 41:89–103, 2015.
- [52] Ravindra K Ahuja. *Network Flow, Transportation and Scheduling: Theory and Algorithms*. Prentice Hall, 1993.
- [53] Thomas H Cormen, Charles E Leiserson, Ronald L Rivest, and Clifford Stein. *Introduction to algorithms*. MIT press, 2009.
- [54] Edsger W Dijkstra. A note on two problems in connexion with graphs. *Numerische Mathematik*, 1(1):269–271, 1959.
- [55] Lester Randolph Ford and Delbert R Fulkerson. Maximal flow through a network. *Canadian journal of Mathematics*, 8:399–404, 1956.
- [56] Ji-Eun Byun, Hee-Min Noh, and Junho Song. Reliability growth analysis of k-out-of-n systems using matrix-based system reliability method. *Reliability Engineering & System Safety*, 165:410–421, 2017.
- [57] Anxin Guo, Zhenliang Liu, Suchao Li, and Hui Li. Seismic performance assessment of highway bridge networks considering post-disaster traffic demand of a transportation system in emergency conditions. *Structure and Infrastructure Engineering*, 13(12):1523–1537, 2017.

## Appendix A. Details of two-component parallel system.

The distance  $\Delta_{12}$  between the two components is given as 11.12 km, and the distances  $R_1$  and  $R_2$  from the epicenter to the two components are given as 3.46 km and 9.28 km, respectively. The seismic capacity parameters for the components are homogeneously assumed to be 0.98 for the median  $\bar{C}_i$ , and 0.69 for the log-standard deviation  $\zeta_i$ .

## Appendix B. Detailed results of numerical examples in Section 4.

### Appendix B.1. Details of two-terminal reliability estimates on the two-component parallel system.

$M_w$	Separate implementations			Single implementation			Exact $P_f$
	$\hat{P}_{f,SS}$	<i>c.o.v.</i>	$N_G$	$\hat{P}_{f,SS}$	<i>c.o.v.</i>	$N_G$	
9.0	$5.38 \times 10^{-2}$	0.110	1,900	$5.37 \times 10^{-2}$	0.108	1,900	$5.34 \times 10^{-2}$
8.5	$3.99 \times 10^{-2}$	0.120	1,900	$3.94 \times 10^{-2}$	0.119	900	$3.94 \times 10^{-2}$
8.0	$2.84 \times 10^{-2}$	0.138	1,900	$2.84 \times 10^{-2}$	0.141	900	$2.85 \times 10^{-2}$
7.5	$2.04 \times 10^{-2}$	0.145	1,900	$2.00 \times 10^{-2}$	0.168	900	$2.02 \times 10^{-2}$
7.0	$1.41 \times 10^{-2}$	0.149	1,927	$1.39 \times 10^{-2}$	0.191	900	$1.40 \times 10^{-2}$
6.5	$9.55 \times 10^{-3}$	0.179	2,465	$9.36 \times 10^{-3}$	0.210	900	$9.49 \times 10^{-3}$
6.0	$6.34 \times 10^{-3}$	0.196	2,791	$6.19 \times 10^{-3}$	0.231	900	$6.31 \times 10^{-3}$
5.5	$4.15 \times 10^{-3}$	0.187	2,800	$4.02 \times 10^{-3}$	0.248	900	$4.10 \times 10^{-3}$
5.0	$2.62 \times 10^{-3}$	0.196	2,800	$2.55 \times 10^{-3}$	0.264	900	$2.60 \times 10^{-3}$
4.5	$1.62 \times 10^{-3}$	0.241	2,840	$1.58 \times 10^{-3}$	0.285	900	$1.62 \times 10^{-3}$
4.0	$1.00 \times 10^{-3}$	0.255	3,290	$0.96 \times 10^{-3}$	0.323	900	$0.98 \times 10^{-3}$
3.5	$5.89 \times 10^{-4}$	0.269	3,682	$5.75 \times 10^{-4}$	0.346	900	$5.85 \times 10^{-4}$
3.0	$3.46 \times 10^{-4}$	0.286	3,700	$3.35 \times 10^{-4}$	0.379	900	$3.40 \times 10^{-4}$
Sum			33,895			12,700	

Appendix B.2. Details of four-terminal reliability estimates on the San Diego highway bridge network.

$M_w$	Single implementation			Three divided implementations			MCS $P_f$
	$\hat{P}_{f,SS}$	<i>c.o.v.</i>	$N_G$	$\hat{P}_{f,SS}$	<i>c.o.v.</i>	$N_G$	
9.0	$5.30 \times 10^{-1}$	0.029	1,000	$5.30 \times 10^{-1}$	0.029	1,000	$5.36 \times 10^{-1}$
8.5	$4.12 \times 10^{-1}$	0.055	900	$4.13 \times 10^{-1}$	0.040	900	$4.13 \times 10^{-1}$
8.0	$3.07 \times 10^{-1}$	0.069	900	$3.06 \times 10^{-1}$	0.055	900	$3.10 \times 10^{-1}$
7.5	$2.19 \times 10^{-1}$	0.086	900	$2.17 \times 10^{-1}$	0.083	900	$2.17 \times 10^{-1}$
7.0	$1.51 \times 10^{-1}$	0.118	900	$1.54 \times 10^{-1}$	0.072	1,000	$1.54 \times 10^{-1}$
6.5	$1.02 \times 10^{-1}$	0.164	900	$1.05 \times 10^{-1}$	0.121	900	$1.05 \times 10^{-1}$
6.0	$6.90 \times 10^{-2}$	0.203	900	$7.15 \times 10^{-2}$	0.196	900	$7.25 \times 10^{-2}$
5.5	$4.71 \times 10^{-2}$	0.252	900	$4.83 \times 10^{-2}$	0.279	900	$4.90 \times 10^{-2}$
5.0	$3.18 \times 10^{-2}$	0.319	900	$3.38 \times 10^{-2}$	0.128	1,900	$3.32 \times 10^{-2}$
4.5	$2.15 \times 10^{-2}$	0.388	900	$2.30 \times 10^{-2}$	0.180	900	$2.28 \times 10^{-2}$
4.0	$1.48 \times 10^{-2}$	0.452	900	$1.58 \times 10^{-2}$	0.262	900	$1.56 \times 10^{-2}$
3.5	$1.01 \times 10^{-2}$	0.512	900	$1.09 \times 10^{-2}$	0.339	900	$1.11 \times 10^{-2}$
3.0	$6.83 \times 10^{-3}$	0.569	900	$7.48 \times 10^{-3}$	0.408	900	$7.56 \times 10^{-3}$
Sum			11,800			12,900	

Appendix B.3. Details of 3-out-of-5 reliability estimates on the San Diego highway bridge network.

$M_w$	Single implementation			Two divided implementations			MCS $P_f$
	$\hat{P}_{f,SS}$	<i>c.o.v.</i>	$N_G$	$\hat{P}_{f,SS}$	<i>c.o.v.</i>	$N_G$	
9.0	$5.96 \times 10^{-1}$	0.026	1,000	$5.96 \times 10^{-1}$	0.027	1,000	$5.94 \times 10^{-1}$
8.5	$4.48 \times 10^{-1}$	0.077	900	$4.48 \times 10^{-1}$	0.045	900	$4.55 \times 10^{-1}$
8.0	$3.08 \times 10^{-1}$	0.094	900	$3.09 \times 10^{-1}$	0.064	900	$3.14 \times 10^{-1}$
7.5	$1.95 \times 10^{-1}$	0.121	900	$1.94 \times 10^{-1}$	0.101	900	$2.03 \times 10^{-1}$
7.0	$1.14 \times 10^{-1}$	0.147	900	$1.14 \times 10^{-1}$	0.135	900	$1.17 \times 10^{-1}$
6.5	$6.31 \times 10^{-2}$	0.196	900	$6.17 \times 10^{-2}$	0.191	900	$6.60 \times 10^{-2}$
6.0	$3.18 \times 10^{-2}$	0.262	900	$3.47 \times 10^{-2}$	0.132	1,900	$3.38 \times 10^{-2}$
5.5	$1.59 \times 10^{-2}$	0.330	900	$1.71 \times 10^{-2}$	0.202	900	$1.67 \times 10^{-2}$
5.0	$7.50 \times 10^{-3}$	0.445	900	$8.26 \times 10^{-3}$	0.337	900	$8.07 \times 10^{-3}$
4.5	$3.44 \times 10^{-3}$	0.587	900	$3.84 \times 10^{-3}$	0.481	900	$3.80 \times 10^{-3}$
4.0	$1.54 \times 10^{-3}$	0.746	900	$1.73 \times 10^{-3}$	0.650	900	$1.69 \times 10^{-3}$
3.5	$6.75 \times 10^{-4}$	0.951	907	$7.87 \times 10^{-4}$	0.818	900	$8.02 \times 10^{-4}$
3.0	$3.05 \times 10^{-4}$	1.154	900	$3.61 \times 10^{-4}$	0.990	904	$3.62 \times 10^{-4}$
Sum			11,807			12,904	